Effects of Buccal Thickness Augmentation on Bone Remodeling after Maxillary Anterior Implantation

Keke Zheng[1], Nobuhiro Yoda[2], Junning Chen[3], Zhipeng Liao[1], Jingxiao Zhong[1], Shigeto Koyama[4], Christopher Peck[5], Michael Swain[1], Keiichi Sasaki[2], and Qing Li*,[1].

[1] School of Aerospace, Mechanical and Mechatronic Engineering, The University of Sydney, NSW 2006, Australia

[2] Division of Advanced Prosthetic Dentistry, Tohoku University Graduate School of Dentistry, 4-1, Seiryo-machi, Aoba-ku, Sendai, Miyagi, 9808575, Japan

[3] College of Engineering, Mathematics, and Physical Sciences, University of Exeter, EX4 4QF United Kingdom

[4] Maxillofacial Prosthetics Clinic, Tohoku University Hospital, 1-1, Seiryo-machi, Aoba-ku, Sendai, Miyagi, 9808575, Japan

[5] Faculty of Dentistry, The University of Sydney, Sydney, NSW, 2006, Australia

Abstract

The biomechanics associated with buccal bone thickness (BBT) augmentation remains poorly understood, as there is no consistent agreement in the adequate BBT to avoid over-loading resorption or over-augmenting surgical difficulty. This study utilizes longitudinal clinical image data to establish a self-validating time-dependent finite element (FE) based remodeling procedure to explore the effects of different buccal bone thicknesses on long-term bone remodeling outcomes *in silico*. Based upon the clinical computed tomography (CT) scans, a patient-specific heterogeneous FE model was constructed to enable virtual BBT augmentation at four different levels (0.5, 1.0, 1.5 and 2.0 mm), followed by investigation into the bone remodeling behavior of the different case scenarios.

The findings indicated that although peri-implant bone resorption decreased with increasing initial BBT from 0.5mm to 2mm, different levels of the reduction of bone loss was associated with the amount of bone augmentation. In the case of 0.5 mm BBT, overloading resorption was triggered during the first 18 months, but such bone resorption was delayed when the BBT increased to 1.5 mm. It was found that when the BBT reached a threshold thickness of 1.5 mm, the bone volume can be better preserved. This finding agrees with the consensus in dental clinic, in which 1.5mm BBT is considered clinically justifiable for surgical requirement of bone graft. In conclusion, this study introduced a self-validating bone remodeling algorithm *in silico,* and it divulged that the initial BBT affects the bone remodeling outcome significantly, and a sufficient initial BBT is considered essential to assure long-term stability and success of implant treatment.

Keywords: Bone remodeling validation, Overloading bone resorption, Buccal bone thickness (BBT), Virtual surgery, Iterative finite element analysis (FEA).

1. Introduction

Along with the popularity of dental implants in prosthodontics, clinical expectation following implant treatment anticipates not only yielding initial stability but also preserving long-term bone volume and maintaining a healthy status of peri-implant tissue. This becomes particularly crucial in the case of implantation with significant anatomical restrictions, such as insufficient bone volume and surgically unfavorable positions, which could potentially lead to severe postoperative bone resorption. In the maxillary anterior region, for example, alignment with native teeth is considered a major priority for implantation (1). However, this often leads to unbalance of bone volume between the buccal and patatel sides of the implant (i.e. thinner bone thickness on the buccal side than patatel region). When the initial bone volume is insufficient, part of the buccal bone could gradually reduce as a result of over-loading resorption over time, along with a further high-risk consequence of soft tissue recession (2). For this reason, the critical buccal bone morphology around an implant is widely considered to be a primary factor to reduce peri-implant bone resorption (2-6). Although the recent clinical studies (7, 8) reported high survival rates of implants inserted in the anterior maxillary bone augmented with mandibular bone grafts, the actual effect of additional bone volume on the long-term bone remodeling activity remains unclear; and there is limited information available to estimate the minimal bone thickness required from the biomechanical perspective.

Clinical CT-based three-dimensional (3D) finite element (FE) models have exhibited compelling advantages in the biomechanical analysis, which allow fairly precisely capturing anatomical features of an individual subject in terms of patient-specific bone morphology and site-dependent heterogeneity of material properties (9, 10). Further, various mechanobiology-based bone remodeling algorithms have been proposed for dental implantology, enabling to understand, predict and manipulate bone adaptation associated with a range of clinical scenarios (11-15). Although few FE-based remodeling studies (15, 16) have investigated how peri-implant tissue responds to different insertion angles and loading directions of implants in the anterior maxillary region, none of them has genuinely considered the influence of grafted buccal bone thickness (BBT). In addition, validation of the remodeling prediction against clinical follow-up is largely missing in the previous remodeling studies, though few recent studies have enabled to validate their simulated remodeling results by generating virtual X-Ray against the clinical X-ray images measured at the same time points (11, 12, 17). Note that in comparison with X-ray imaging, computed tomography (CT) imaging is more sophisticated by featuring its 3D nature that provides more thorough non-invasive longitudinal data for validating the simulated bone remodeling process *in silico*.

Considering the above challenges, this study aimed to (1) establish a finite element based bone remodeling procedure to associate the mechanobiological stimulus modeled *in silico* with the change of bone density measured in clinical follow-up *in vivo*; and (2) explore the effects of different buccal bone thicknesses (BBTs) on long-term outcome of bone remodeling. It is hypothesized that increase of BBT would improve bone remodeling and preservation thanks to alleviation of over-loading resorption. This study demonstrates that the combined *in-vivo* clinical follow-up and *in-silico* FE remodeling algorithm establishes an effective framework to examine and predict time-dependent activities of bone turnover subject to different clinical options in maxilla, thereby evaluating and enabling surgical planning for the minimal buccal bone required, thus ensuring stability and longevity of implantation treatment.

2. Materials and Methods

2.1. Clinical data acquisition and analysis

In this study, a 52-year-old female was recruited, following the treatment of maxillary right incisor fracture in Tohoku University Hospital in Japan. A titanium implant (Osseospeed TX

3.5S, DENTSPLY Implants, Mölndal, Sweden), with a 3.5mm diameter and 13.0mm length, was inserted after a healing period of 8 weeks. The cone-beam (CB) CT scan (3D Accuitomo, MORITA Corp., Kyoto, Japan) was performed at a standardized exposure of 90 kV and 35 mA at 0 month (T0), 6 months (T1), 12 months (T2) and 18 months (T3) after implantation. An initial buccal bone thickness (BBT) was measured and found to be 0.25mm. It is noted that direct loading in the implant region was avoided over the first six months. Since this study focused on biomechanically-driven bone remodeling following the initial healing process, the starting time point (T1) was selected to be month six after implantation. Besides, there was no sign of infection observed around the implant in this experimental course, which allows us to restrict our attention to the biomechanical aspect behind in this study.

3D image registration was carried out to quantify the longitudinal changes of bone surface profile and mineral density by using Amira 2016.22 (Zuse Institute Berlin (ZIB), Berlin, Germany). The implant was selected to be the reference geometry because of its rigidity and high contrast. As shown in Fig. 1, the region of interest (ROI) around the implant was divided into four sectors (namely SegB, SegM, SegP, and SegD), starting from the position that is 45° away from either x or y-axis, which prescribed its origin in the center of mass of the implant (Fig. 1b). In each set of CTs, 52 slices that cover the implant region were selected, and thereby 208 ROIs were generated for a specific time point. To characterize the variation in bone mineral density (BMD) in the peri-implant area along the axial direction of implant, the variation of greyscale in the ROIs was measured with respect to the distance from the implant neck to the apex. The average voxel intensity (i.e., greyscale) was calculated in the cortical bone region of each slice (at a regular spacing of 0.25 mm along the coronal axis), enabling us to plot the change of pixel value in the axial direction.

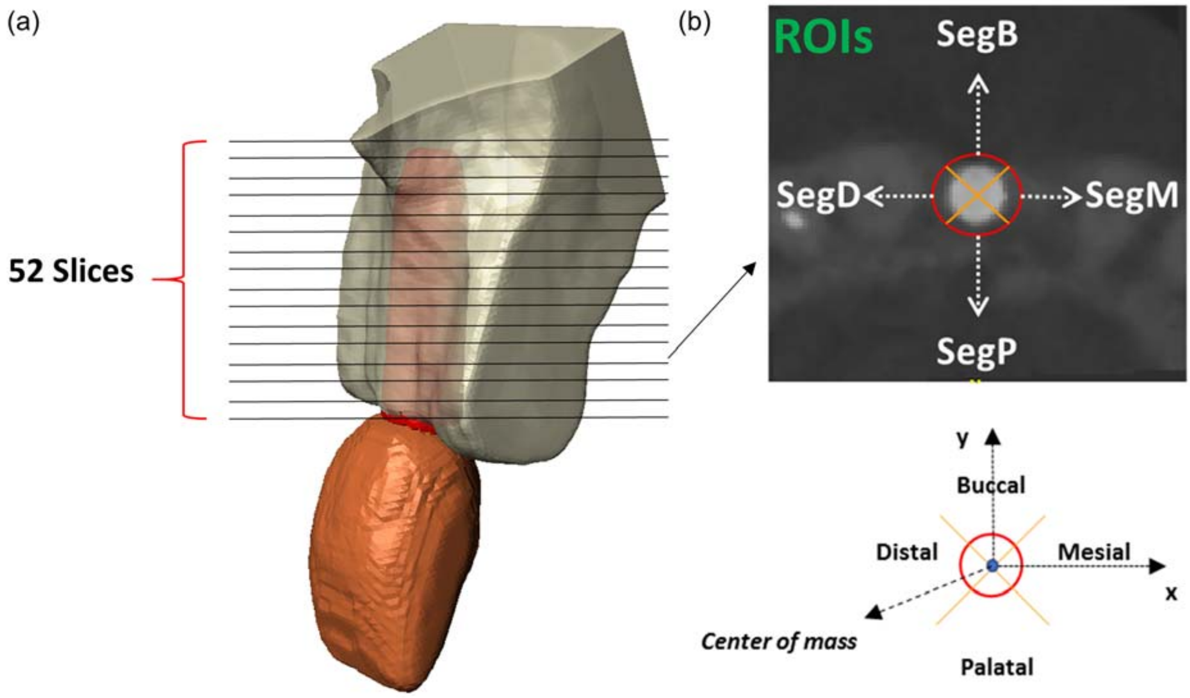

Fig. 1 Procedure for identification of the region of interest (ROI) and illustration of the orientation in this study: The peri-implant region was covered in the 52 slices (a), four sectors were divided in each slice to represent ROIs in the different directions (b), based upon the coordinates generally accepted in dental clinics.

2.2 Finite element (FE) modeling

The 3D FE models were created for this specific patient based upon the CT scan data obtained at time point T1. ScanIP Ver. 4.3 (Simpleware Ltd, Exeter, UK) was used for segmentation and Rhinoceros 4.0 (Robert McNeel & Associates, Seattle, USA) was used for parametrization of the reconstructed models with non-uniform rational B-spline (NURBS) representation. Following the development of the maxilla model with detailed dentition, the implant with abutment and screw was modeled in SolidWorks 2015 (SolidWorks Corp, Waltham, MA, USA), as shown in Fig. 2a. In the peri-implant region, the cylindrical ROI described in the previous section was created (Fig. 2b).

Using virtual morphological modification in ScanIP, four different buccal bone thicknesses were created by augmenting from the baseline model (T1) to replicate the extent of bone grafting in the buccal bone region, with an increment of 0.5 mm in Rhinoceros. The specific buccal bone region was determined as the rectangular area covered by the length of the dental implant and the breadth of the intra-implant-tooth distance (the green square-shaped area in Fig. 2e).

In this study, site-dependent material heterogeneity was assigned to model the maxillary bone by characterizing the bone density as per localized Hounsfield Unit (HU). This allowed to more precisely capture the anatomic variation of bone density and modulus, which could considerably affect biomechanical responses (Fig. 2c) (9, 11). Teeth and dental implants were assumed to be linear elastic. All the material properties adopted in this study are summarized in Table 1.

A masticatory force was set to be 38.3 N. This value was obtained from the measured force *in vivo* by crushing a peanut through a single implant-supported crown at the maxillary incisor region (18). The load transfer angle was set to be 65º to the long axis of the implant, as measured between the upper and the lower incisor tooth axes in the cast model of the patient (Fig. 2b). Full constraints were prescribed on the sectioned regions that were considered remote from the loading point (Fig. 2d).

Table 1. Material properties adopted in FE models (Yoda et al 2017)

Materials	Young's Modulus (MPa)	Poisson's ratio
Bone	Heterogeneous	0.30
Bone Graft	14,000	0.3
Periodontal ligament (PDL)	Hyperelastic (Marlow)	0.45
Teeth (enamel and dentine)	20,000	0.20

Titanium (Implant, abutment, screw)	110,000	0.35
Ceramic crown	140,000	0.28

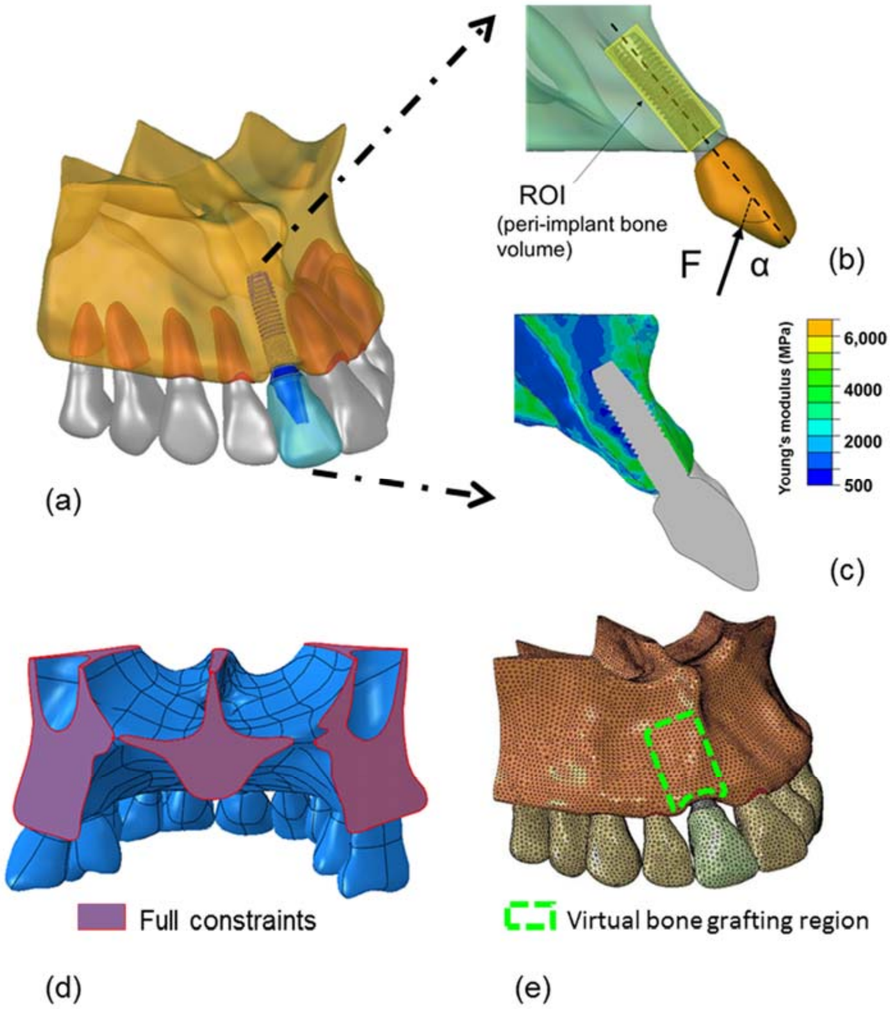

Fig. 2 Procedure for FE model construction: (a) solid models of the maxilla and implant; (b) region of interests (ROIs) in the peri-implant and loading condition: F = 38.3 N, α = 65 degrees; (c) site-specific material properties of osseous tissues assigned in terms of Hounsfield Unit (HU) values obtained from the clinical CBCT data through a FORTRAN subroutine in ABAQUS; (d) kinematic boundary conditions; and (e) virtual bone grafting region

The final assemblies were exported to ABAQUS 6.13.1 (Dassault Systèmes, Tokyo, Japan) for the FE analysis. An adaptive mesh was generated, and a mesh convergence test was conducted to ensure numerical accuracy. The final model comprised of 301,108 10-node quadratic tetrahedral elements, with 9,033,240 degrees of freedoms (DoF). An assumption of complete bone - implant contact (BIC), implying full osseointegration status, was assigned (14, 19, 20). The implant components, including implant body, screw, abutment, and superstructure were assumed to be perfectly bonded for simplification, as the micromotions between these components were not the primary interest of this study.

2.3. Bone remodeling algorithm

The FE-based bone remodeling prediction requires the biomechanical responses of site-dependent units (e.g., elements) within the bone by determining the mechanical stimuli generated by external loads. Once the mechanical stimulus deviates to a certain extent from the specific homeostatic level, the bone will respond by adapting its morphology (21, 22). In the literature, the strain energy density (SED) per unit apparent density has been widely accepted as an appropriate mechanical stimulus for bone remodeling of dental bones (22-24), which is defined by

$$\Xi = \frac{U}{\rho} \tag{1}$$

where parameters U, ρ and Ξ are the SED (J/cm^3), local bone density (g/cm^3) and mechanical stimulus (J/g), respectively.

The remodeling algorithm relates the changing rate of the apparent bone density to the differences between mechanical stimulus and physiological threshold K (23). As the mechanical stimulus increases, three phases of remodeling outcomes can be resulted namely; underloading bone resorption, bone equilibrium, bone apposition (25, 26). Note that the greater the mechanical stimulus, the higher the rate of density change, which does not necessarily correlate to the clinical scenarios where severe damage can be caused if loading is excessively higher than a critical value for physiological self-repair in the bone. Therefore, a quadratic term was introduced to the bone apposition phase once the mechanical stimulus exceeds a specific level (24). In summary, the density increment ($\Delta\rho$) over a time interval (Δt) can be calculated as,

$$\Delta\rho = \begin{cases} C_{ap}[\Xi - K(1+s)]\Delta t - C_{or}[\Xi - K(1+s)]^2\Delta t; & if\ \Xi > K(1+s) \\ 0; & if\ \ K(1-s) \le \Xi \le K(1+s) \\ C_{ur}[\Xi - K(1-s)]\Delta t; & if\ \ \Xi < K(1-s) \end{cases} \qquad (2)$$

where the reference stimulus $K = 0.00036\ (J/g)$ (Lin et al. 2010c) and $2s = 0.2$ is the width of the lazy zone doe the dental bones (Rungsiyakull et al. 2011). C_{ap}, C_{or} and C_{ur} are the rate constants for bone apposition, overloading resorption and underloading resorption, respectively. All these rate constants were determined by using an inverse identification approach during the model validation against the longitudinal historic data acquired from clinical follow-up, the details of which will be described in the following section. The minimum and maximum densities of bone were set to be 0.7 g/cm^3 and 1.9 g/cm^3, respectively (Lin et al. 2010c). The time step in this study represented 1 month, thereby 48 iterations were set in total here.

The remodeling procedure was implemented through a FOTRAN subroutine (UMAT) in ABAQUS, where the material properties of bone in each element were evaluated as per the user-defined constitutive models. A flowchart that presents the bone remodeling procedure is depicted in Fig. 3. To more appropriately quantify the variations in bone density and mechanical stimulus within each ROIs, their volume average was calculated as:

$$\rho = \frac{1}{V}\int_V \rho dV \cong \frac{\sum_{e=1}^{n} \rho_e V_e}{\sum_{e=1}^{n} V_e}$$

$$\Xi = \frac{1}{V}\int_V \Xi dV \cong \frac{\sum_{e=1}^{n} \Xi_e V_e}{\sum_{e=1}^{n} V_e} \qquad (3)$$

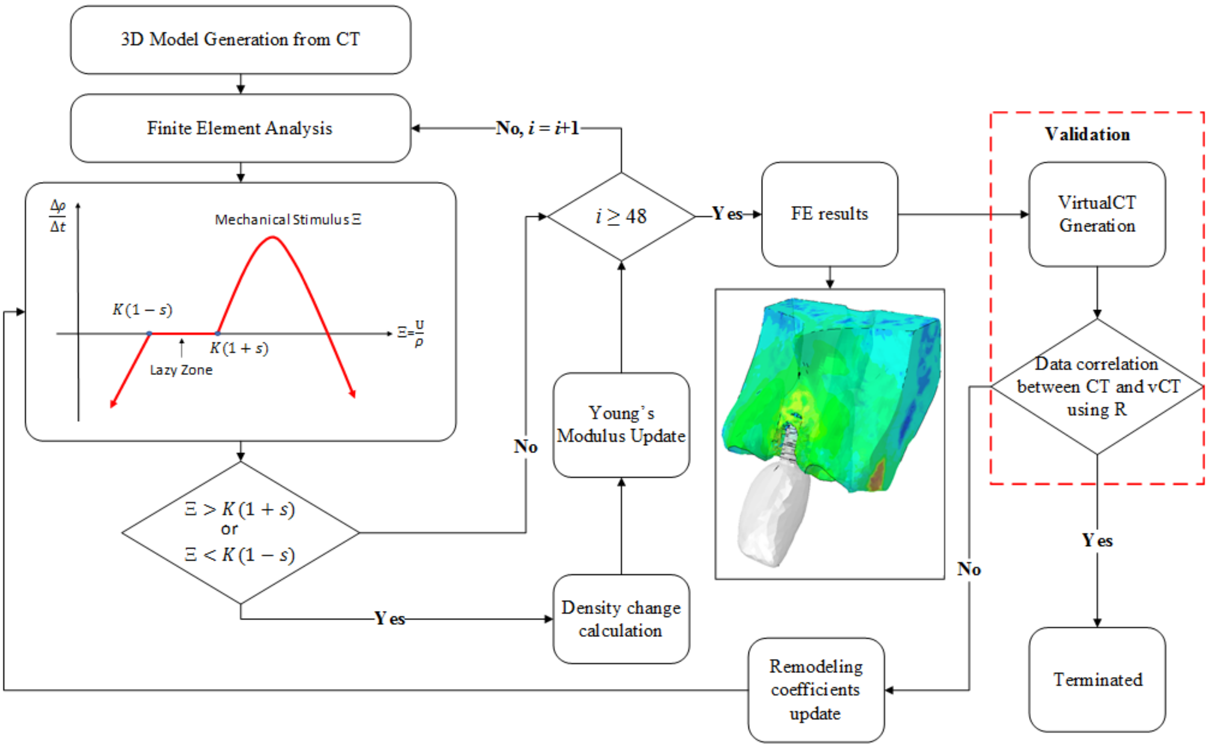

Fig. 3 Flowchart of the FE-based bone remodeling algorithm and the procedure of correlation with clinical follow-up

2.4. Bone remodeling validation

To validate the remodeling outcome, the FE-based virtual CT images were generated from the simulated densities at the time points T1, T2, and T3, respectively. A python program, namely pxyCT was used to convert the simulated results into virtual CTs (12), which were correlated with the clinical follow-up in a quantitative fashion. As aforementioned, the virtual CT stacks were aligned with the corresponding clinical CT images at the same time point. As such, the virtual *in-silico* simulated CTs and real *in-vivo* clinical CTs were compared in the identical ROIs. At each time point, these 208 ROIs were correlated (Fig. 4).

The time-dependent changes of mean grayscale values in these ROIs were calculated based upon both virtual CT and clinical CT using MATLAB (MathWorks, Inc., Massachusetts, USA).

A linear regression analysis was performed by using Graph-Pad Prism 7 (GraphPad Software, Inc. CA,USA) to evaluate the coefficients of determination (R^2), coefficients of correlation (R) and p-values. The R^2 and R were calculated for assessing the correlation between the simulated and clinical data, in terms of the changes in the bone grayscale values in all ROIs at different time points. The p values were calculated to test the null hypothesis that the overall slope of the fitted line is zero. It should be noted that the linear regression was implemented for any two time periods, e.g., T12 (i.e. from time point T1 to time point T2) and T13 (from T1 to T3), for a better clinical relevance (27).

By regulating the bone resorption and apposition rates, one set of remodeling parameters in Eq. (2), which provides the best possible correlation between the grayscale value in the simulated remodeling results and clinical data in all the ROIs, was finally selected. Specifically, C_{ap}, C_{or} and C_{ur} were set to be 5.1 month g/cm^5, 6000 month^3 g/cm^7 and 5.1 month g/cm^5, respectively.

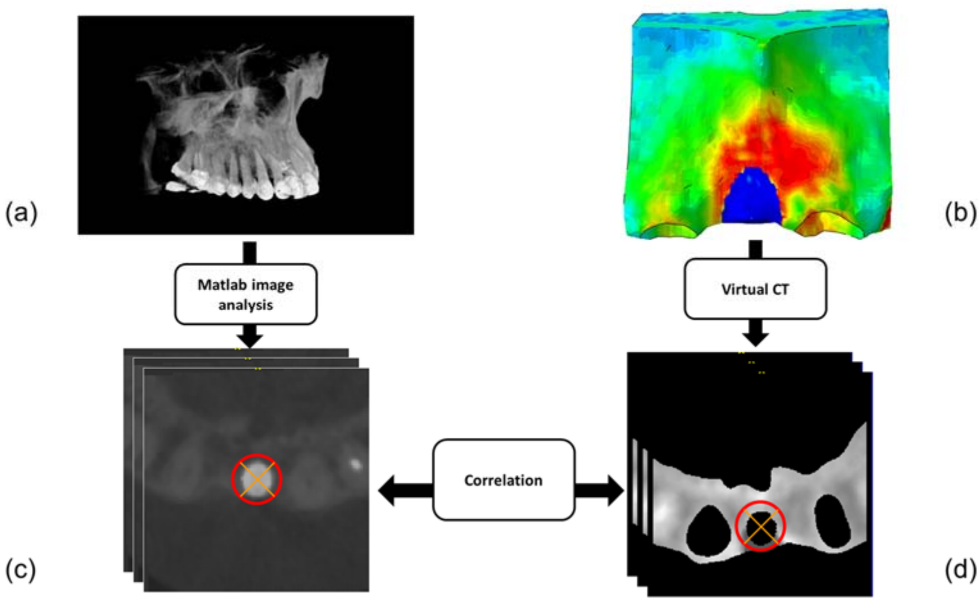

Fig. 4 Procedure of validating bone remodeling algorithm against clinical follow-up: firstly, a python program called pxyCT was used to convert the simulated density model (right upper) to a stack of virtual CT images (right lower). To be noted, since only one bone region was focused on, other anatomical structures such as teeth and PDLs, were excluded in this process. Secondly, the same ROIs dividing process (as illustrated in Fig. 1) was

performed on both sets of images in Matlab, to quantify the volume-averaged densities for correlation between the real clinical CT (left) and virtual simulated CT images.

3. Results

3.1. Bone remodeling validation

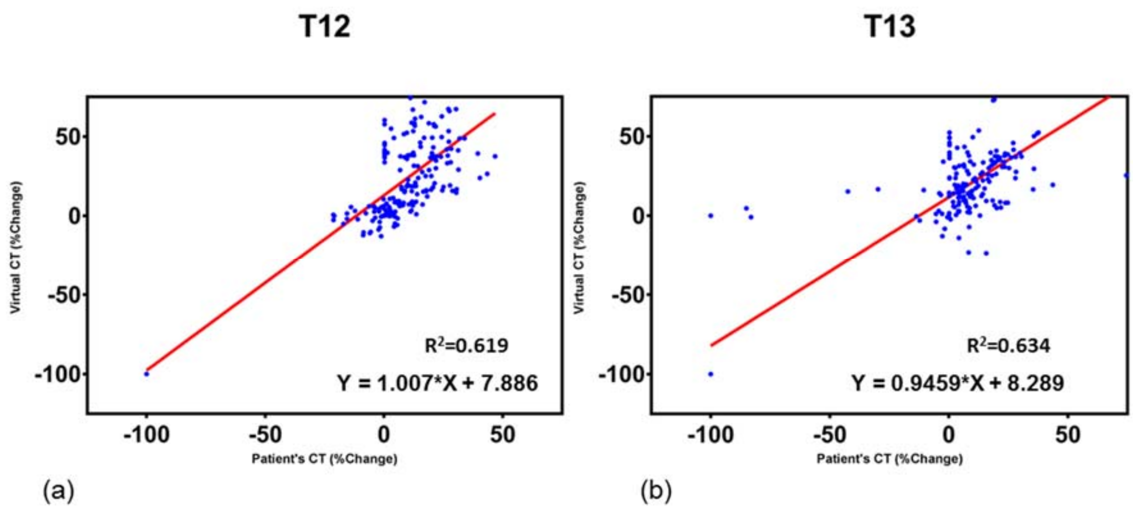

Fig. 5 Linear regression analysis between the timeframe changes of ROI grayscale in the real clinical CT and virtual simulated CT, for (a) T12 (T1 to T2) and (b) T13 (T1 to T3).

The correlations between the clinical CT and FE virtual CT images at the two time periods (i.e. T1 to T2 and T1 to T3, respectively) are shown in Fig. 5. As described, the linear regressions between the density changes (%) in ROIs were carried out in both the images sets. Specifically, the R^2 values from the multi-stage remodeling procedure were evaluated to be 0.619 and 0.634 for T12 and T13, respectively, with the p values less than 0.001. Therefore, a proper correlation was obtained between the simulated bone remodeling *in silico* and the clinical follow-up *in vivo* (28).

3.2. Images based assessment of bone mineral density

The contours of simulated bone resorption were compared with the surface model generated from the clinical CT images at time points T1, T2 and T3 (Fig. 6 a-b). By regulating the remodeling parameters for matching the clinical follow-up data, a similar trend of bone resorption was observed between these two sets of data, in which the buccal bone covering the implant neck was seen to resorb from time T2 and continued until almost one-third of the implant was directly exposed at time point T3. More specifically, from the clinical CT results it is observed and quantified that bone resorption started from the neck region then propagated towards the apical area of the implant along the axial direction of the implant (Fig. 6c-f). By looking at the buccal and palatal regions of the implant, sector SegB underwent more severe resorption than sector SegP. The buccal bone line (SegB) moved towards the implant apex by 1.75mm and 4 mm at T2 and T3, respectively; whereas this movement was only 0.5mm and 2mm in the palatal region (SegP). Meanwhile, in the medial (SegM) and distal (SegD) regions, the extent of bone resorption was less than that in SegB and SegP.

In contrast to the neck region, bone remodeling around the implant from the body to apex is far milder. Interestingly, the shape of the density variation curve in SegB differs with the others that all have an evident drop in the density. This is due to the fact that the implant was inserted into the position required to align it with the other native teeth, which necessitated the implant to be placed close to the buccal side, making the region SegB mostly cortical bone. In the other regions, the average bone density drops in the cancellous regions (Fig. 6 d-f). The overall distributions of bone density at the different time points exhibit fairly close resemblance between the real clinical CT images and simulated virtual CT images in all these four regions, except that there is a certain delay of the bone resorption rate. In region SegB, the simulated bone resorption progressed to 1.5mm and 3.5mm from the implant neck region at time points T2 and T3, respectively, which differed by around 0.25mm and 0.5mm from the clinical CT data. Considering the overall correlation of the density distributions between the FE virtual CT and clinical CT data, such errors are at an acceptable level.

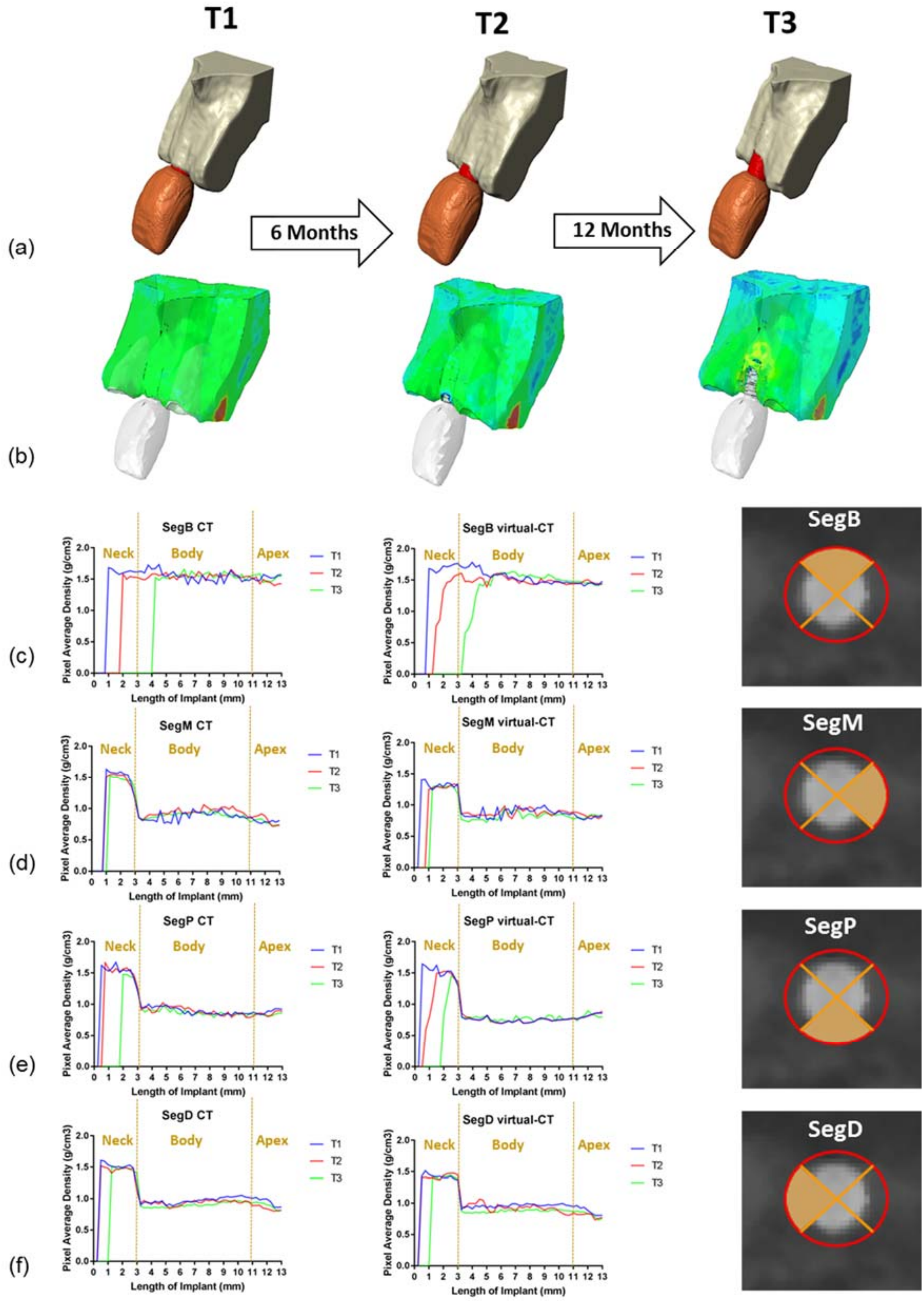

Fig. 6 Illustrative and quantitative comparison on bone remodeling at the three time points (i.e. T1, T2 and T3) for both clinical CT and simulated results: the illustrative comparison of the three time points has been conducted for (a) surface models generated from clinical CT images and (b) contours of density distribution from the

simulated models. Afterward, a quantitative comparison on the bone density distribution curves along the implant axis was performed in the four specific regions, such as (c) SegB, (d) SegM, (e) SegP and (f) SegD. In each region, the density distribution around the implant from the neck towards the apex were quantified from the both clinical (right) and simulated (left) data.

3.3. BBT effects on remodeling outcome

Since bone grafting allows the surgeon to generate a range of buccal bone thicknesses (BBTs) before implantation, four different BBTs (named as BBT05, BBT10, BBT15, and BBT20, representing 0.5, 1.0, 1.5 and 2.0mm buccal bone thicknesses) were modeled in this study (upper row in Fig. 7a). A palatal-buccal sectional view was selected for comparing the mechanical stimulus and density contours of the buccal and palatal bone areas for these different BBTs. Strain energy density (SED) distributions are provided in the lower row of Fig. 7a as an example of mechanical stimuli. From the contour of BBT05 (thickness = 0.5mm), it can be seen that the buccal side generated substantially higher SED than the palatal side, which was associated with the direction of the occlusal force and amount of the bone volume for bearing the occlusal load. As BBT increased, nevertheless, the concentration of SED on the crestal bone region decreased.

As shown in Fig. 7b, the density contours as the simulated results of bone remodeling at the four-time points (i.e., months 12, 24, 36 and 48) are presented for the different BBTs. Note that month 6 (T1) was selected to be the initial time point for the remodeling simulation, as the direct loading started only from this time point. For clearer observation of the bone resorption, density was considered to be zero when it fell below 0.1g/cm^3 and was displayed in dark gray area. In the original model (BBT05), evident resorption started on the buccal bone in the neck region and propagated along the implant axis direction. However, the resorption plateaued in the both regions after month 24. Meanwhile, the bone resorption on the palatal side appeared to be slower in comparison with the other side from month 24 to month 48. Whilst bone apposition was observed in the buccal bone region around the implant body, from month 36 to month 48.

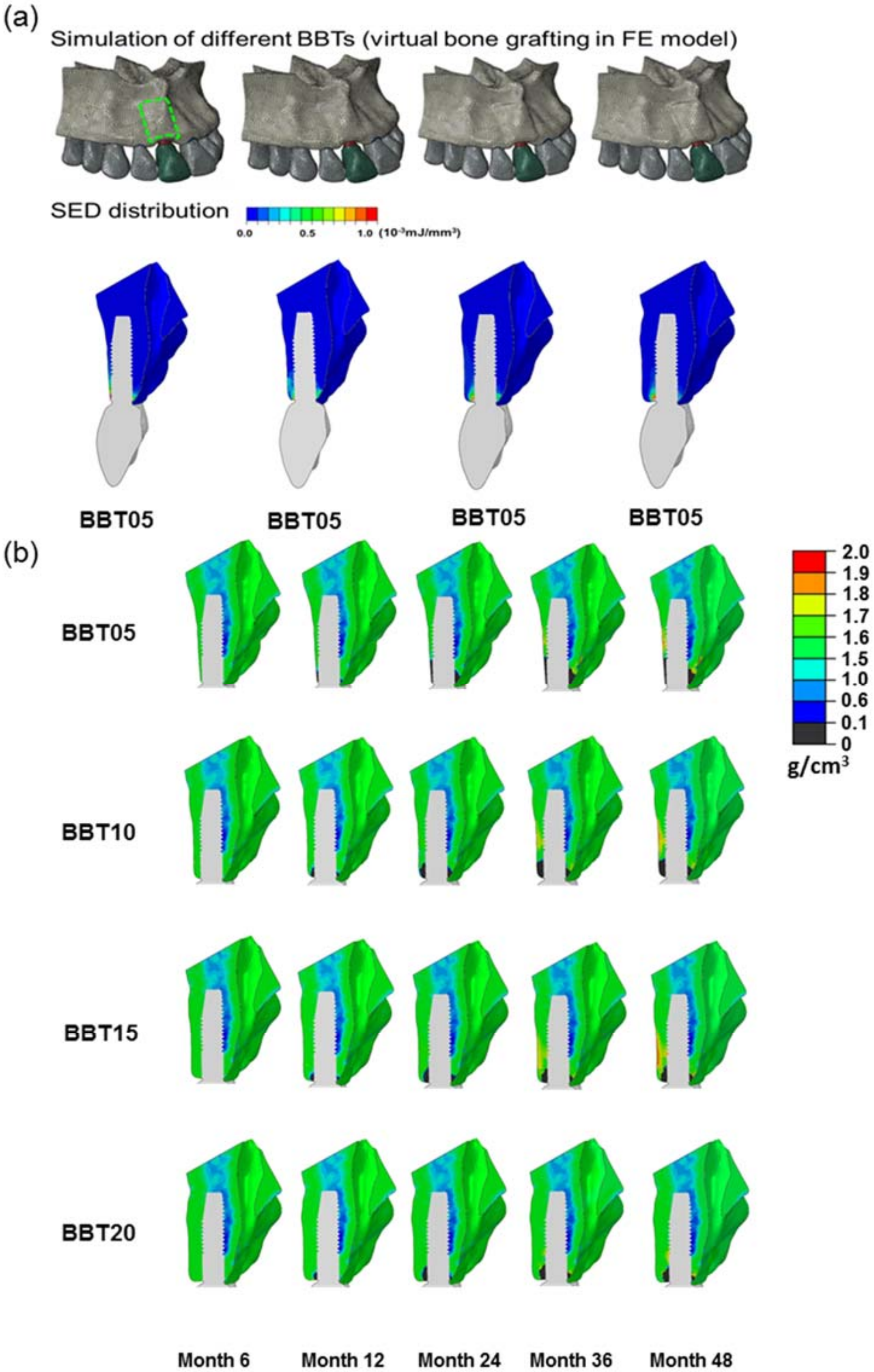

Fig. 7 The mechanical stimuli in a buccal bone area with different BBTs. (a) FE models (upper row) and the examples of SED distribution (lower row) based upon the simulated bone grafting strategy; (b) cross-sectional images of buccal bone on the implant for investigating the distribution of density in different BBTs.

When BBT increased, the overall density contour retained a similar pattern, except for the local area around the implant neck, where a decrease of the resorption rate can be observed on the both buccal and palatal sides in the course from month 6 to month 48. When the BBT was set to be 1.5mm (BBT15), the bone resorption that initiated from the bone-implant contact (BIC) area was restricted from extending to the buccal bone surface. Comparison between BBT05, BBT10 and BBT15, exhibited a similar pattern, but in a larger magnitude, of bone apposition from month 24 to month 48. Interestingly, bone apposition was not seen in BBT20. This is due to the fact that the buccal bone region was too thick, and the bone surface is too far away from the loading point, meaning that the load and associated strain energy may not be uniformly distributed across such a thick bone section. Apart from the buccal side, the bone resorption on the palatal side decreased as the BBT increased. Interestingly, it is found that in the regions where bone resorption plateaued, bone apposition was still observed, acting as a barrier to prevent bone resorption from further progression.

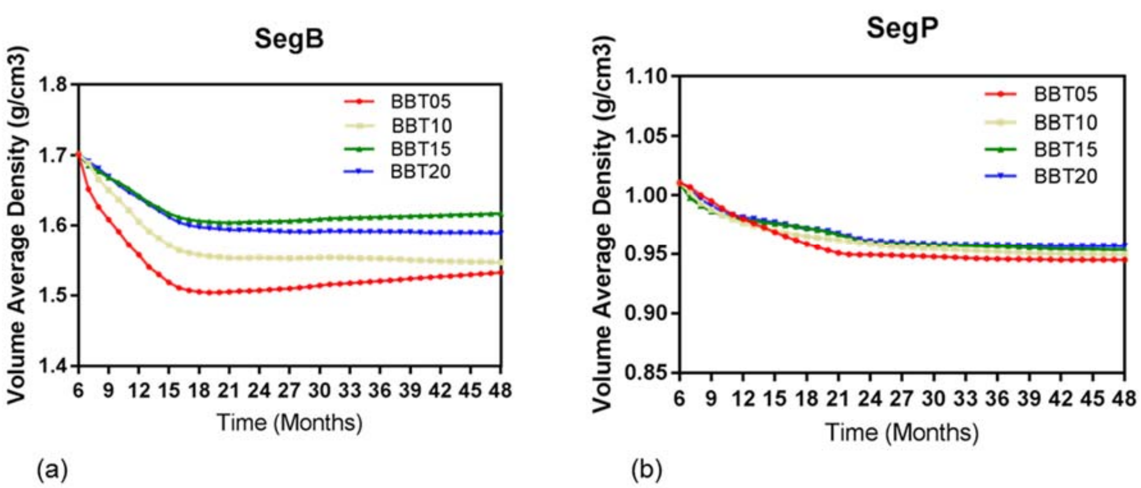

Fig. 8 Remodeling progress of (a) SegB, and (b) SegP region over the 48 months.

The collective quantification of bone remodeling in regions SegB and SegP are compared for the different BBTs in Fig. 8, because the buccal and palatal regions of the implant attracts the most attention in clinic (27). For the SegB region, the simulated remodeling process developed relatively faster from 6 to 16 months; but such a process appears to become stable in the following months. It is interesting to note that after month 21, the overall density progressively increased till month 48 while the resorption in the SegP region progressed continuously from month 6 to month 21 until the remodeling process was leveled off.

Regarding the effect of BBT variation, overall density was seen to substantially increase on the buccal side (SegB) when the BBT increased from 0.5mm to 1.5 mm. However, when BBT reached 2.0 mm, the density decreased. On the opposite side (SegP), the overall density increased as the BBT increased, but no noticeable difference can be seen between BBT15 and BBT20. In other words, an increase in BBT from 0.5mm to 1.5mm successfully decelerated the resorption rate for both the regions; but an increase from 1.5 mm to 2.0 mm led to almost the same trend of remodeling, meaning that there was no significant difference of remodeling progression between BBT15 and BBT20, except that BBT15 has more density increase on the buccal side after month 18. On the opposite region (SegP), a similar trend of bone remodeling was observed to that in SegB, except for the relatively small variation between the different BBTs. In this region, the overall density decreased from BBT05 to BBT15 and became stable without further change between BBT15 and BBT20.

4. Discussion

Recently, there has been an increasing concern on progressive resorption on the buccal bone above the implant in the anterior maxilla (1, 29-31). Clinically, this consequence may lead to insufficient bone volume for maintaining functionality and esthetics following implantation treatment. In contrast to the other efforts dedicated to investigation specifically into the influence of implant inclinations, little attention has been paid to the effects of buccal bone resorption (BBT) on consequent changes in bone volume and density around an implant so far. Therefore, in this study, a clinically validated bone remodeling algorithm was first developed for evaluating the long-term remodeling process in a patient-specific fashion by involving the effects of different BBTs.

4.1. Remodeling outcome

Although various mechanobiology-driven bone remodeling algorithms have been proposed and utilized for dental implantation analysis (22), the remodeling parameters, especially the rate constants that regulate the overall remodeling progress, vary widely within the literature as they have been derived from different human tissues, patient groups and research methodologies. Therefore, a proper correlation between the remodeling simulation results and corresponding clinical follow-up data is required for validating the bone remodeling algorithm to ensure reliable prediction results.

Compared with the previous studies that focused on specific regions (e.g. the regions with clinical significance) for correlating with clinical data (11, 12), ROIs used in this study were generated by dividing the entire peri-implant region into four representative segments with a specific number of image slices. Considering a slice interval of 0.25mm, 208 ROIs were generated in this study to cover the bone around the whole implant (13mm), which provided more thorough spatial quantification of the remodeling information.

It is noted that in this specific case, buccal bone resorption started from the onset of the remodeling process (Fig. 8a) but decelerated overtime during the remodeling process. In general, two types of bone resorption can be specified, which are associated with underloading or overloading resorptions respectively (24). Crupi et al (2004) found that excessive marginal bone loss correlated well with the presence of overload. Other studies indicated that bone remodeling can be driven by micro-damage induced by a certain level of loading (32). It is noteworthy noting that excessive load generated around implants can impair osseointegration

(33), thus decreasing peri-implant bone density and leading to the occurrence of crater-like defects (34).

According to Eq. (2), underloading resorption initiates when mechanical stimulus $\varXi$ is below the lower threshold $K(1-s)$, and apposition is triggered when $\varXi$ passes the upper threshold $K(1+s)$; whereas when $\varXi$ passes a critical upper limit, overloading resorption may take place. As the resorption was originated from the crestal bone region around the screw threads, where the highest SED appeared, the risk of the overloading resorption was high. For this specific case, the initial buccal bone volume was considered insufficient for achieving a proper long-term survivorship of implantation.

As shown in Fig. 8, although dramatic bone resorption was observed during the first few months of loading and the resorption rate decreased as time passed. Furthermore, at month 18, bone resorption plateaued, and was followed by bone apposition till month 48. This is due to the fact that when the bone density decreased to a level below 0.1 g/cm^3, such region was unable to provide mechanical support to the occlusal load. As a consequence, the loading region in buccal bone that withstood the maximum loading from the implant was shifted from the neck to the middle region under the same loading condition; this lower SED was accumulated in the supporting region. Therefore, in this case, the resorption rate decreased as a result of the bone resorption progressed.

On the other hand, the bone resorption progressed faster on the buccal side than that on the palatal side, which agrees well with the relevant clinical studies reported in literature (35). The possible causes are attributable to the direction of the applied occlusal load (36) and different initial bone volume available to support the implant. Due to the asymmetry of the bone around the implant axis, the buccal side has less bone in comparison with the palatal side. Thus, the SED distributions in the buccal and palatal regions are asymmetric. Specifically, the buccal region exhibits a higher SED in response to the transverse loading as a result of its lower bone volume relative to the palatal region (Fig. 8a). This is due to the fact that there was less bone volume on the buccal side for bearing mechanical loading.

Since SED was considered to be the mechanical stimulus for driving remodeling simulation, the higher SED distributed on the buccal bone due to its less supporting bone volume and the inherent direction of occlusal loading (i.e. towards to the buccal side), faster resorption rate was observed than the other side. Also, such finding directs more attention to the consequence of changing BBTs on remodeling outcomes.

4.2. Effect of BBT on the mechanical stimuli

Since resorption occurred after initial occlusal loading, the presence of sufficient buccal bone volume at implant placement is considered to be one of the essential factors for preventing bone resorption under loading. According to the simulated results, the apportion rate was seen to decrease on the buccal side. This arises because as buccal bone volume increases, the SED concentration decreases as more bone volume is available for withstanding occlusal loads. As a result, the mechanical stimuli in the peri-implant region were found to be lower in the thicker BBT (Fig. 8a), suggesting a significant role played by BBT on redeploying mechanical stimuli in the peri-implant regions. However, from BBT15 to BBT20, bone resorption rates showed the minimal difference in the first 15 months (Fig. 8a). This can be explained by the reduction of the SED magnitude when the BBT reached a certain amount, where the extra bone volume has limited benefit to the alleviation of the SED concentration.

Interestingly, from month 18 onwards, all the four models with the different BBTs experienced bone apposition for the remainder of the period. As shown in Fig. 8b, except for BBT20, evident bone appositions can be seen in the buccal bone above the mid-region of the implant at month 36 and month 48. As the bone apposition started from the buccal surface, a possible explanation can be that the stress caused by the bending moment from the occlusal force was concentrated in this region. Unlike the other three models, BBT20 has an extra bone volume on the buccal side which provided sufficient bending support from the occlusal force. In other words, more bone volume there to withstand stress under the same loading condition reduced the overall stress concentration at the “bending spot”, i.e., the region substances major load under bending. Thus, no significant bone apposition occurred for that specific region. In general, when BBT reached 1.5mm, remodeling outcomes were substantially improved in comparison with the original stage, in terms of both bone resorption reduction and bone apposition.

4.3. Clinical implication and limitations

As a pilot study of using a time-dependent FEA procedure to investigate the long-term effect of BBT on the bone remodeling, the present findings were in good agreement with the clinical data available in literature. Through a clinical CBCT analysis of an anterior maxillary implant, Veltri et al. showed that buccal bone resorption occurred in the neck region of the implant (i.e., thin bone area) in most cases (1). They also found that the implant with the greatest bone resorption was associated with a smaller buccal bone volume in the coronal portion and thinner bone, both buccally and marginally. Needless to say, a thicker bone is more ideal for implantation. Clinically, it is well accepted that 1.5mm is a sufficient thickness for the bone augmentation (27). If the native BBT is more than 1.5 mm, the implant placement can be carried out without bone augmentation. Otherwise, it is necessary to perform bone grafting before implantation. The findings in the present study are in good agreement with current clinical consensus that BBT of 1.5 mm appears to be a threshold value for determining the pre-surgical bone thickness.

There are some inherent limitations in this patient-based study. First, while the specific patient was modeled to establish a conceptual assessment framework accounting for buccal bone responses, all the interfaces between different tissue/materials were assumed to be fully bonded and osseointegrated completely after a 6 month healing period. This assumption will affect the transfer of occlusal load to the bone around an implant. There is a need to develop a proper algorithm to model the bone-implant contact (BIC) interaction in a time-dependent manner. Second, further follow-up observations and data collection of this patient are still needed to obtain more detailed longer-term results of the bone remodeling. Third, the remodeling parameters were obtained for this specific patient and a larger number of patient samples is certainly required to gain broader popularity and confidence on this topic. Nevertheless, these abovementioned factors were beyond the scope of the present paper, further research will help clarify the biomechanical responses induced by implant treatment more realistically.

5. Conclusions

This study developed a computational procedure to assess the effects of buccal bone thickness (BBT) on the bone remodeling outcome in a time-dependent fashion by correlating simulated remodelling *in silico* with the clinical follow-up *in vivo*. The simulated remodeling results of apparent bone density were converted into virtual CT image data and then quantitatively correlated with the corresponding clinical CT data over one and half year duration of clinical follow-up. The strong correlation provided sufficient confidence and credibility for the proposed FE based remodeling algorithm. Importantly, this patient-specific validation approach provided us with a procedural tool to explore individualized bone remodeling outcome for surgical planning. For this particular patient, the simulated results revealed that increasing the initial BBT could decrease the bone resorption in the peri-implant region, and when BBT reached 1.5mm, it is considered to achieve a safe condition for implantation surgeries.

Acknowledgements

This study was supported by Australian Research Council (ARC) through Discovery scheme (DP160104602). We greatly appreciate Dr Michael Hogg for the invention of the open-source pyvCT package.

Conflict of interest

Authors have no conflict of interest concerning the present manuscript.

Reference

1. Veltri M, Ekestubbe A, Abrahamsson I, Wennström JL. Three-Dimensional buccal bone anatomy and aesthetic outcome of single dental implants replacing maxillary incisors. Clinical oral implants research. 2015.

2. Grunder U, Gracis S, Capelli M. Influence of the 3-D bone-to-implant relationship on esthetics. Int J Periodontics Restorative Dent. 2005;25(2):113-9.

3. Nisapakultorn K, Suphanantachat S, Silkosessak O, Rattanamongkolgul S. Factors affecting soft tissue level around anterior maxillary single-tooth implants. Clinical oral implants research. 2010;21(6):662-70.

4. Merheb J, Quirynen M, Teughels W. Critical buccal bone dimensions along implants. Periodontology 2000. 2014;66(1):97-105.

5. Teughels W, Merheb J, Quirynen M. Critical horizontal dimensions of interproximal and buccal bone around implants for optimal aesthetic outcomes: a systematic review. Clinical oral implants research. 2009;20(s4):134-45.

6. Tanasić I, Tihaček-Šojić L, Mitrović N, Milić-Lemić A, Vukadinović M, Marković A, et al. An attempt to create a standardized (reference) model for experimental investigations on implant's sample. Measurement. 2015;72:37-42.

7. Kuchler U, von Arx T. Horizontal ridge augmentation in conjunction with or prior to implant placement in the anterior maxilla: a systematic review. International Journal of Oral & Maxillofacial Implants. 2014;29.

8. Pieri F, Nicoli Aldini N, Marchetti C, Corinaldesi G. Esthetic outcome and tissue stability of maxillary anterior single-tooth implants following reconstruction with mandibular block grafts: a 5-year prospective study. International Journal of Oral & Maxillofacial Implants. 2013;28(1).

9. Chen J, Ahmad R, Suenaga H, Li W, Swain M, Li Q. A comparative study on complete and implant retained denture treatments–a biomechanics perspective. Journal of biomechanics. 2015;48(3):512-9.

10. Ahmad R, Abu-Hassan MI, Li Q, Swain MV. Three dimensional quantification of mandibular bone remodeling using standard tessellation language registration based superimposition. Clinical oral implants research. 2013;24(11):1273-9.

11. Field C, Li Q, Li W, Thompson M, Swain M. Prediction of mandibular bone remodelling induced by fixed partial dentures. Journal of biomechanics. 2010;43(9):1771-9.

12. Liao Z, Yoda N, Chen J, Zheng K, Sasaki K, Swain MV, et al. Simulation of multi-stage nonlinear bone remodeling induced by fixed partial dentures of different configurations: a comparative clinical and numerical study. Biomech Model Mechanobiol. 2016:1-13.

13. Lin D, Li Q, Li W, Duckmanton N, Swain M. Mandibular bone remodeling induced by dental implant. Journal of biomechanics. 2010;43(2):287-93.

14. Rungsiyakull C, Chen J, Rungsiyakull P, Li W, Swain M, Li Q. Bone's responses to different designs of implant-supported fixed partial dentures. Biomech Model Mechanobiol. 2015;14(2):403-11.

15. Wang C, Zhang W, Ajmera D, Zhang Y, Fan Y, Ji P. Simulated bone remodeling around tilted dental implants in the anterior maxilla. Biomech Model Mechanobiol. 2015:1-12.

16. Hsu M-L, Chen F-C, Kao H-C, Cheng C-K. Influence of off-axis loading of an anterior maxillary implant: a 3-dimensional finite element analysis. International Journal of Oral & Maxillofacial Implants. 2007;22(2).

17. Field C, Li Q, Li W, Swain M. Influence of tooth removal on mandibular bone response to mastication. Archives of Oral Biology. 2008;53(12):1129-37.

18. Svensson KG, Trulsson M. Impaired force control during food holding and biting in subjects with tooth‐or implant‐supported fixed prostheses. Journal of clinical periodontology. 2011;38(12):1137-46.

19. Chen J, Ahmad R, Suenaga H, Li W, Swain M, Li Q. A comparative study on complete and implant retained denture treatments–A biomechanics perspective. Journal of biomechanics. 2014.

20. Chen J, Rungsiyakull C, Li W, Chen Y, Swain M, Li Q. Multiscale design of surface morphological gradient for osseointegration. Journal of the Mechanical Behavior of Biomedical Materials. 2013;20(0):387-97.

21. Frost HM. Wolff's Law and bone's structural adaptations to mechanical usage: an overview for clinicians. 2009.

22. Lin D, Li Q, Li W, Swain M. Dental implant induced bone remodeling and associated algorithms. Journal of the Mechanical Behavior of Biomedical Materials. 2009;2(5):410-32.

23. Weinans H, Huiskes R, Grootenboer HJ. The behavior of adaptive bone-remodeling simulation models. Journal of Biomechanics. 1992;25(12):1425-41.

24. Li J, Li H, Shi L, Fok AS, Ucer C, Devlin H, et al. A mathematical model for simulating the bone remodeling process under mechanical stimulus. dental materials. 2007;23(9):1073-8.

25. Frost HM. Bone's mechanostat: a 2003 update. The Anatomical Record Part A: Discoveries in Molecular, Cellular, and Evolutionary Biology. 2003;275(2):1081-101.

26. Huiskes R, Weinans H, Grootenboer H, Dalstra M, Fudala B, Slooff T. Adaptive bone-remodeling theory applied to prosthetic-design analysis. Journal of biomechanics. 1987;20(11):1135-50.

27. Yoda N, Zheng K, Chen J, Li W, Swain M, Sasaki K, et al. Bone morphological effects on post-implantation remodeling of maxillary anterior buccal bone: A clinical and biomechanical study. Journal of prosthodontic research. 2017;61(4):393-402.

28. Norman GR, Streiner DL. Biostatistics: the bare essentials: Bc Decker Hamilton; 2008.

29. Benic GI, Mokti M, Chen CJ, Weber HP, Hämmerle CH, Gallucci GO. Dimensions of buccal bone and mucosa at immediately placed implants after 7 years: a clinical and cone beam computed tomography study. Clinical oral implants research. 2012;23(5):560-6.

30. Degidi M, Nardi D, Daprile G, Piattelli A. Buccal bone plate in the immediately placed and restored maxillary single implant: a 7-year retrospective study using computed tomography. Implant dentistry. 2012;21(1):62-6.

31. Tan Z, Kang J, Liu W, Wang H. The effect of the heights and thicknesses of the remaining root segments on buccal bone resorption in the socket‐shield technique: An experimental study in dogs. Clinical implant dentistry and related research. 2018;20(3):352-9.

32. Lee T, Staines A, Taylor D. Bone adaptation to load: microdamage as a stimulus for bone remodelling. Journal of Anatomy. 2002;201(6):437-46.

33. Ali B, Meddah HM, Merdji A. Effects of overloading in mastication on the mechanical behaviour of dental implants. Materials & Design. 2013;47:210-7.

34. Kitamura E, Stegaroiu R, Nomura S, Miyakawa O. Biomechanical aspects of marginal bone resorption around osseointegrated implants: considerations based on a three‐dimensional finite element analysis. Clinical oral implants research. 2004;15(4):401-12.

35. Al-Shabeeb MS, Al-Askar M, Al-Rasheed A, Babay N, Javed F, Wang H-L, et al. Alveolar bone remodeling around immediate implants placed in accordance with the extraction socket classification: a three-dimensional microcomputed tomography analysis. Journal of periodontology. 2012;83(8):981-7.

36. Tanasić I, Šarac D, Mitrović N, Tihaček-Šojić L, Mišković Ž, Milić-Lemić A, et al. Digital Image Correlation Analysis of Vertically Loaded Cylindrical Ti-Implants With Straight and Angled Abutments. Experimental Techniques. 2016;40(4):1227-33.